The passivation of calcite by acid mine water. Column experiments with Fe(III)-SO_4-H^+ and Fe(III)-Cl-H^+ solutions at pH 2.

Josep M. Soler [ab*], Marco Boi [ab], José Luis Mogollón [ac], Jordi Cama [ab], Carlos Ayora [ab], Peter S. Nico [d], Nobumichi Tamura [d], Martin Kunz [d]

[a] Institute of Earth Sciences "Jaume Almera" (CSIC), Lluís Solé i Sabarís s/n, 08028 Barcelona, Catalonia, Spain

[b] Institute of Environmental Assessment and Water Research (CSIC), Jordi Girona 18, 08034 Barcelona, Catalonia, Spain

[c] Instituto de Ciencias de la Tierra, Universidad Central de Venezuela, Caracas 1020-A, Venezuela

[d] Lawrence Berkeley National Laboratory, 1 Cyclotron Road, Berkeley, CA 94720, USA

[*]Corresponding author
jsoler@ija.csic.es, Ph.: +34 934095410, Fax: +34 934110012

Abstract

Column experiments, simulating the behavior of passive treatment systems for acid mine drainage, have been performed. Acid solutions (HCl or H_2SO_4, pH 2), with initial concentrations of Fe(III) ranging from 250 to 1500 ppm, were injected into column reactors packed with calcite grains at a constant flow rate. The composition of the solutions was monitored during the experiments. At the end of the experiments (passivation of the columns), the composition and structure of the solids were measured.

The dissolution of calcite in the columns caused an increase in pH and the release of Ca into the solution, leading to the precipitation of gypsum and Fe-oxyhydroxysulfates (Fe(III)-SO_4-H^+ solutions) or Fe-oxyhydroxychlorides (Fe(III)-Cl-H^+ solutions). The columns worked as an efficient barrier for some time, increasing the pH of the circulating solutions from 2 to ~ 6-7 and removing its metal content. However, after some time (several weeks, depending on the conditions), the columns became chemically inert. The results showed that passivation time increased with decreasing anion and metal content of the solutions. Gypsum was the phase responsible for the passivation of calcite in the experiments with Fe(III)-SO_4-H^+ solutions. Schwertmannite and goethite appeared as the Fe(III) secondary phases in those experiments. Akaganeite was the phase responsible for the passivation of the system in the experiments with Fe(III)-Cl-H^+ solutions.

Keywords: Acid mine drainage, treatment, calcite, schwertmannite, goethite, gypsum, akaganeite , armoring

1. Introduction

Acid mine drainage (AMD) arising mainly from the oxidation of pyrite and other sulfide minerals is a major environmental problem in many countries (e.g. Kaufmann et al., 1992; Banks et al., 1997; Olías et al., 2004). AMD solutions are characterized by their strong acidity and high concentrations of sulfate, Fe, Al and associated trace metals such as Zn, Cu, Pb, Ni, Co and Cd (e.g. Nordstrom and Alpers, 1999; Cravotta, 2008). Release of contaminants can persist for decades or centuries after mining has stopped.

Engineering designs for AMD passive treatment systems have been developed since the 1990s (Younger, 2000; Younger et al., 2002; Zimkiewicz et al., 2003). A basic feature of these systems is that they do not need continuous addition of reactants and only require limited maintenance. The most common passive treatment systems for AMD are Anoxic Limestone Drains (ALD; Turner and McCoy, 1990) and Reducing and Alkalinity Producing Systems (RAPS; Kepler and McCleary, 1994).

An ALD consists of a trench filled with limestone (calcite) gravel through which AMD flows isolated from atmospheric oxygen. The main alkalinity producing process is the dissolution of calcite. The alkalinity is used in subsequent aeration and sedimentation ponds to oxidize, hydrolyze and precipitate metals (mainly Fe). ALD can only treat reduced, ferrous iron-dominated AMD with less than about 1 ppm Al, Fe(III) or O_2. When exposed to larger concentrations, ALDs tend to clog due to precipitation of Al-hydroxides in the pore space of the system (e.g. Robbins et al., 1996; Watzlaf et al., 2004), or they lose reactivity due to precipitation of Fe hydroxides and hydroxysulfates on the surface of the limestone grains (passivation or armoring; e.g. Pearson and McDonnell, 1975; Santoro et al., 1987; Hammarstrom et al., 2003; Watzlaf et al., 2004).

RAPS have an additional layer of compost or other organic material on top of the limestone layer in order to overcome the limitations of ALDs. The compost layer produces anoxic conditions, which reduce Fe(III) to Fe(II) or limit oxidation of Fe(II) and inhibit passivation of the calcite layer. Sulfate reducing bacteria also generate additional alkalinity. Nevertheless, clogging and passivation also occur in RAPS (Rees et al., 2001; Watzlaf et al., 2002; Ziemkiewicz et al., 2003; Rose et al., 2004; Watzlaf et

al., 2004), especially when high concentrations of Al and/or Fe(III) are present in the inflowing water.

Recently, Rötting et al. (2008a,b) have proposed the use of Dispersed Alkaline Substrate systems (DAS), which make use of calcite sand mixed with a coarse inert matrix (e.g. wood chips). They have shown that larger Fe(III) and Al concentrations can be treated with this system, but coating of calcite grains by gypsum and clogging by Al-precipitates still occur.

To target the issue of loss of reactivity due to coating of the reactive grains or clogging of porosity, column experiments were performed using calcite sand and synthetic acid solutions that contained only Fe(III)-SO_4^{2-}-H^+ or Fe(III)-Cl^--H^+ as major components. Fe(III)-Cl^--H^+ solutions were used to try to isolate the effect of sulfate in these systems. The acid solutions were continuously injected into the calcite-filled columns until calcite dissolution and metal retention stopped taking place. Experiments were performed at pH 2, which corresponds approximately to the most acidic conditions found in acid mine drainage.

2. Experimental methods

Acid solutions (HCl or H_2SO_4, pH 2), with initial concentrations of Fe(III) ranging from 250 to 1500 ppm, were injected into column reactors packed with calcite grains at a constant flow rate. The composition of the effluent solutions was monitored during the experiments. pH was checked every 1 to 2 days; solution chemistry (Fe, S, Mg, Ca, Al, Si) was analyzed at several times (4 to 20) during the experiments. At the end of the experiments (passivation of the calcite in columns), the effect of metal and anion concentration in the solutions on neutralization efficiency was investigated. The evolution of mineralogy and pore structure has been investigated by X-ray diffraction (XRD), Scanning Electron Microscopy (SEM), Electron Microprobe analyses (EM), synchrotron X-ray microtomography (mCT) and synchrotron X-ray microdiffraction (mXRD).

2.1. Analytical methods

Solution composition (Fe, S, Mg, Ca, Al, Si) was measured by Inductively Coupled Plasma – Atomic Emission Spectrometry (ICP-AES), using a Thermo-Jarrel Ash spectrometer equipped with a CID detector. The detection limits for Fe, S, Mg, Ca, Al and Si were 1.8×10^{-7}, 3.5×10^{-6}, 10^{-5}, 5×10^{-6}, 7.5×10^{-7} and 7×10^{-7} mol·l^{-1}, respectively. Error associated with ICP-AES measurement was estimated to be around 3%. Solution pH was measured during the experiment with a Crison© combined glass electrode at room temperature (22 ± 2 ºC) with an error of ±0.02 pH units. The electrode was calibrated regularly with buffer solutions at pH 2 and 7.

X-ray diffractometry (XRD) was performed with a Bruker D-5005 diffractometer using Cu K-α1 radiation (λ=1.5406 Å) at 40 kV and 40 mA. Usually, the range of 2θ scanning was from 4^o to 60^o, with a scan step of 0.05^o and a step duration of 3 s. Standard grinding and mounting of the sample was performed prior to XRD.

Scanning Electron Microscopy (SEM) was performed on C-coated samples using a Hitachi H-4100FE instrument under a 15 to 20 kV potential. Electron Microprobe (EM) analyses were performed on multiple points using a CAMECA SX50 microprobe under a 20 kV accelerating potential and 15 nA beam current.

X-ray microtomography (mCT) images were taken at beamline 8.3.2 of the Advanced Light Source at Lawrence Berkeley National Laboratory. Images were taken at X-ray energy of 40keV using a superbend magnet source and a multilayer monochromator. The small-diameter columns (1.5 cm outer diameter) were mounted on a rotary stage and images were collected every 0.25 degrees through a full 180 degree rotation. Transmitted X-ray light was converted to visible light using a $CdWO_4$ single crystal scintillator, magnified by a Cannon 2X lens, and imaged on a Cooke PCO 4000 CCD camera with a final pixel size of 4.4 microns. Three exposures of 200 ms each were averaged together for a total of 600 ms exposure per image. Nine dark images (with X-ray shutter closed) and twenty-five open beam images (with sample removed form beam) were taken at the end of the data collection and used for background subtraction and normalization. Raw images were reconstructed using the Octopus commercial software package (Dierick et al., 2004).

X-ray microdiffraction (mXRD) was tested on a single thin section from one of the experiments. The measurements were performed on beamline 12.3.2 at the Advanced Light Source. The instrument uses Kirkpatrick-Baez optics to focus the monochromatic X-ray beam delivered by the synchrotron superconducting magnet source down to a size of about 15x2 μm^2 at the sample position. The sample was mounted on a precision XY stage and illuminated with a 8 keV (λ = 1.55 Å) monochromatic X-ray radiation at an incidence angle of 10º. Iron X-ray fluorescence signal was also collected using a Si-drift Vortex detector. X-ray microdiffraction patterns were obtained using a MAR133 X-ray CCD detector. The CCD was set to an angle of $2\theta = 40º$ at a distance of 119 mm from the sample. The exposure time per point for the diffraction patterns was 200 s. The signal collection time per point for fluorescence was 0.2 s.

2.2. Columns

The columns were made from transparent polymethyl methacrylate (PMMA, Fig.1), with inner diameters ranging from 1.2 to 6.4 cm and lengths ranging from 2.5 to 7 cm (Table 1). The smallest columns (diameter < 6 cm) included a bed of glass spheres at top and bottom that was used to homogenize the influent and effluent solutions. The thickness of the bed was about 8 mm and the glass spheres were 2 mm in diameter. Some of the longest columns had 2 additional lateral ports in order to measure pH gradients along the column. Three-way medical valves were used to connect ports and tubing. Solutions were injected from bottom to top with a peristaltic pump under a constant flow rate. Fluid flux ranged from about $5.2x10^{-4}$ to $1.4x10^{-3}$ $l/m^2/s$.

Limestone sand was obtained from the Roca Quarry in the Garraf area (Barcelona). XRD profiles showed only calcite peaks. Acid (pH 2) dissolution of the limestone showed that the molar Ca/Mg ratio was about 80. Si and Al were below detection limit (ICP-AES). Two different ranges of grain size were used for the experiments: (1) 2-5 mm, (2) 1-2 mm. Limestone was already supplied from the quarry in these grain size ranges. Before packing the grains into the columns, the limestone sand was (a) washed with de-ionized water several times until clear output water was obtained, and (b) dried at room temperature.

Porosity was calculated from the known mass of limestone in the columns, the density of calcite (2.71 g/cm^3) and the volume of the columns. Initial porosities ranged between 0.39 and 0.59 (Table 1).

After the experiments, epoxy resin was injected in some of the columns. Slices were cut from these columns for SEM, EM and mXRD analyses.

2.3. Solutions

To prepare the input solutions, appropriate amounts of $FeCl_3$ or $Fe_2(SO_4)_3$ were weighed and dissolved in Millipore MQ water (18 μmhos·cm^{-1}). pH was adjusted to 2 by adding HCl or H_2SO_4. All reactants were analytical (pro analysi) grade.

3. Results

After injection of the acid solutions into the columns, the dissolution of calcite caused an increase in pH and the release of Ca into the solution, leading to the precipitation of gypsum and Fe-oxyhydroxysulfates (Fe(III)-SO_4-H^+ solutions) or Fe-oxyhydroxychlorides (Fe(III)-Cl-H^+ solutions). The monitoring of output solution chemistry in the experiments showed that in early time stages, as input solution flowed through the columns, pH increased from 2 to ~ 6 -7. After some time (Fig.2a, Table 1) output pH dropped abruptly to values close to 2 (pH < 3) and Ca concentrations decreased (limited by equilibrium with respect to gypsum in the case of Fe(III)-SO_4-H^+ solutions). Fe(III) output concentrations remained very low (usually total conc. including colloids < 10 ppm) as far as output pH was larger than 5.

Output pH showed two different behaviors with time. For Cl^- solutions, after the first pH drop occurred, short-lived transitory rises of pH were observed (Fig. 2a). They were probably linked to the removal and transport of fine-grained precipitates (Fe-oxyhydroxychlorides), exposing fresh calcite surfaces to solution. For SO_4^{2-} solutions, once pH dropped it remained close to input values for weeks.

pH profiles were also measured along some of the longest columns, making use of intermediate sampling ports. pH values showed variations with time that followed the visually observed advance of the reaction fronts (coating of the grains with brown-orange precipitates) and the temporary reactivations (Fig. 2).

Figures 3ac show the time needed to passivate the columns (drop in pH at the column outlet), normalized to residence time (τ) in the column, vs. Fe(III) and anion input concentrations. As expected, there is a clear trend towards decreasing passivation times with increasing concentrations for input Fe(III) less than 1000 ppm (about a ×20 decrease in t/τ for a ×4 increase in Fe or for a ×2.5 increase in equivalents of SO_4/Cl). The same plots are also given in terms of maximum amount of Fe(III) retained (passivation time × flow rate × input concentration) by the columns in Figs. 3bd. The trend towards decreasing amounts of retained metal with increasing input concentrations can be observed, but the plots show an increase for Fe(III) input concentrations larger than 1000 ppm.

Comparison of Figs. 3ac and 3bd shows that the almost constant passivation time for large input concentrations (horizontal trend at high concentrations in Figs. 3ac) translates into a larger amount of metal retained (passivation time × flow rate × input concentration). The opposite effect can be observed for low concentrations (horizontal trend at 250 ppm Fe(III) in Figs. 3bd). Error is dominated by the time between pH measurements (each data point corresponds to the first measurement after the drop in pH, i.e. the maximum possible passivation time).

Figure 3 also shows a trend towards larger retention of metal and longer passivation times with decreasing grain size. When using the smaller grain size (× and O symbols in Fig. 3), passivation times and amount of Fe(III) retained are larger. This trend is only broken by experiment F (Fe(III)-SO_4-H^+ solution, 1000 ppm Fe, solid square symbol), and it may be caused by the large grain size (2-5 mm) relative to column diameter (4 cm) in the experiment. The other experiments using limestone sand of the same grain size were conducted with columns with larger diameters (6.4 cm).

Notice that the trends in passivation time or amount of Fe(III) retained correlate with both Fe(III) and anion concentrations in the influent solution. However, the analysis of

the reacted solids allowed the identification of the chemical components responsible for the passivation of the calcite.

Examination of the reacted columns by Scanning Electron Microscopy showed the formation of coatings on the original calcite grain surfaces. Figure 4 shows an SEM image and a Fe elemental map from a section from column 4 (Fe(III)-Cl-H^+ solution, 1500 ppm Fe). The large grains are limestone, and the Fe elemental map shows clearly the formation of precipitates on the surface. XRD allowed the detection of akaganeite (FeO(OH,Cl)) in these experiments. Minor amounts of goethite and hematite were also detected.

Figure 5 shows an SEM image and elemental maps from a section from column δ (Fe(III)-SO_4-H^+ solution, 1000 ppm Fe). The images clearly show the presence of gypsum directly coating the calcite grain surfaces, and Fe-precipitates towards the center of the pores between calcite grains. The elemental maps also show that the Fe-precipitates contain some sulfur. XRD allowed the detection of gypsum and schwertmannite in these experiments (Fig. 6). However, schwertmannite proved to be very difficult or impossible to identify in most of the columns, due probably to its low crystallinity. Notice also that the Fe-precipitates contribute significantly to the filling of the pores, which may eventually cause major changes in permeability.

Electron Microprobe analyses performed on samples from 2 columns (column δ, 1000 ppm Fe, and a column at 500 ppm Fe stopped before passivation) showed that the composition of the Fe(III) precipitates was characterized by variable Fe/S molar ratios. 23 measurements were made, providing a range of Fe/S between 5 and 20. Small amounts of Ca and Si were also detected. Ca/S and Si/S ranged between 0 and 1.7, except for one point with Si/S = 5.

X-ray microtomography images of small-diameter (1.2 cm) columns reacted with Fe(III)-SO_4-H^+ solutions (500, 1000, 1500 ppm Fe) clearly showed the precipitation of gypsum directly on the calcite grain surfaces, while Fe-containing phases precipitated further away from those surfaces (towards the center of the pores). Gypsum is always the mineral phase coating the calcite grain surfaces and causing the passivation of the

columns. Figure 7 corresponds to a section from column δ (Fe(III)-SO_4-H^+ solution, 1000 ppm Fe). Calcite grains (lighter gray) are coated by gypsum (darker gray). Fe-precipitates are brighter. The formation of preferential pathways for the flow was also evident (areas without any indication of reaction are caused by lack of flow).

X-ray synchrotron microdiffraction was tested on a single thin section from column F (Fe(III)-SO_4-H^+ solution, 1000 ppm Fe). Fig 8a shows an optical micrograph of the sample. The area represented by the red rectangle was scanned under the focused X-ray beam to collect the iron Kα fluorescence signal, which confirmed that the darkest areas in the image correspond to the Fe-precipitates. X-ray microdiffraction patterns were recorded at the locations indicated in Fig 8a. Calcite, gypsum and goethite were the phases identified in points 1, 2 and 3 (Fig. 8b), respectively. No evidence of schwertmannite was found in this thin section. The transformation of schwertmannite into goethite with time may have played a role during the experiments (weeks to months). This time scale would be sufficient for this transformation to take place, at least partially (Acero et al., 2006).

4. Discussion and conclusions

Column experiments, simulating the behavior of passive treatment systems for acid mine drainage, have been performed. Acid solutions (HCl or H_2SO_4, pH 2), with initial concentrations of Fe(III) ranging from 250 to 1500 ppm, were injected into column reactors packed with calcite grains at a constant flow rate. The composition of the solutions was monitored during the experiments. At the end of the experiments (passivation of the columns), the composition and structure of the solids were measured with different techniques (XRD, SEM, EM analyses, mCT, mXRD).

The dissolution of calcite in the columns caused an increase in pH and the release of Ca into the solution, leading to the precipitation of gypsum and Fe-oxyhydroxysulfates (Fe(III)-SO_4-H^+ solutions) or Fe-oxyhydroxychlorides (Fe(III)-Cl-H^+ solutions). The columns worked as an efficient barrier for some time, increasing the pH of the circulating solutions from 2 to ~ 6-7 and removing its metal content. However, after some time (several weeks, depending on the conditions), the columns became

chemically inert. Temporary reactivations of the columns (increase in pH) could be observed in the experiments with Fe(III)-Cl-H^+ solutions.

The results showed that gypsum is the phase responsible for the coating of the calcite grains and passivation of the columns in the experiments with Fe(III)-SO_4-H^+ solutions at pH 2. The trends shown in Fig. 3 (decrease in passivation time and amount of metal retained with increasing input concentrations) are not due to the larger Fe(III) concentrations, but to the larger SO_4 concentrations instead (more efficient uptake of the Ca released by the dissolving calcite by the precipitating gypsum). This trend is consistent with the results obtained by Huminicki and Rimstidt (2008). They showed, using batch experiments, that the formation of gypsum coatings on calcite surfaces at a given pH depended on SO_4 concentration. Sulfate concentrations will be a key parameter to take into account when designing barrier systems, given the large sensitivity of barrier lifetime to input concentrations. Additionally, a smaller size of the limestone grains translates into larger passivation times.

In the experiments with Fe(III)-SO_4-H^+ solutions, schwertmannite was detected as the main Fe(III) precipitate in some of the experiments, but it was not detected in many other cases, due probably to its low crystallinity. Goethite was detected in other cases. The transformation of schwertmannite into goethite with time may have played a role during the experiments (weeks to months). This time scale would be sufficient for this transformation to take place, at least partially.

In the experiments with Fe(III)-Cl-H^+ solutions, the phase responsible for the passivation of the calcite grains was a Fe(III) oxyhydroxychloride (akaganeite). Unlike in the experiments with Fe(III)-SO_4-H^+ solutions, the concentration of Fe(III) in the input solution must have a direct effect on the passivation of the calcite, since there was no other phase coating the grains. Similar results were reported by Santomartino and Webb (2007), although in their experiment (pH 4.2, ferrous iron, concentrations of Fe(II), K, SO_4 and Cl in the order of 100 ppm) the Fe(III) precipitates were goethite and lepidocrocite.

The fact that the experiments with Fe(III)-SO_4-H^+ solutions do not show the temporary reactivations observed with the Fe(III)-Cl-H^+ solutions is most probably due to the

strong attachment of gypsum onto calcite surfaces (Booth et al., 1997; Huminicki and Rimstidt, 2008 and references within). Santomartino and Webb (2007) noted the presence of a void (up to 60 μm wide) between the Fe(III) precipitates and the limestone surfaces in their experiments (precipitates could be dislodged).

The Fe(III)-precipitates in the experiments do contribute significantly to the filling of the pores of the medium. Permeability may be reduced to a significant extent in those cases, greatly affecting the efficiency of the barrier systems. This effect may possibly be greater when using smaller grain sizes (larger total reactive area). The column experiments reported here were performed under constant flow rate, imposed by a peristaltic pump. Although the decrease in permeability was never large enough to cause a decrease in flow rate in the experiments, this effect cannot be properly quantified from the results.

All the experiments were performed at pH 2, which corresponds approximately to the most acidic conditions and highest sulfate concentrations found in acid mine drainage. Future experiments will address the behavior of this system under higher pH and smaller sulfate concentrations.

Acknowledgments

We wish to express our gratitude to Fermí Roca (Roca Quarry) for providing the limestone samples, to Eva Pelegrí and Xavier Llovet from the Scientific-Technical Services of the University of Barcelona for their helpful assistance in the ICP-AES and EM analyses, to Josep Elvira (Inst. Jaume Almera) for the XRD work, and to Carl Steefel and Alastair MacDowell for assistance in organizing the work at Lawrence Berkeley National Laboratory. The reviews of the manuscript by C. Cravotta and D. Rimstidt are also acknowledged. Research was funded by projects CTM2006-28151-E/TECNO and CTM2007-66724-C02-01/TECNO from the Spanish Ministry of Science. The Advanced Light Source is supported by the Director, Office of Science, Office of Basic Energy Sciences, of the U.S. Department of Energy under Contract No. DE-AC02-05CH11231.

References

Acero, P., Ayora, C., Torrentó, C., Nieto, J.-M., 2006. The behavior of trace elements during schwertmannite precipitation and subsequent transformation into goethite and jarosite. Geochimica et Cosmochimica Acta 70, 4130-4139.

Banks, D., Younger, P.L., Arnesen, R.T., Iversen, E.R., Banks, S.B., 1997. Mine-water chemistry: the good, the bad and the ugly. Environmental Geology 610 32, 157-174.

Biedermann, G., Chow, J.T., 1966. Studies on the hydrolysis of metal ions. The hydrolysis of the iron(III) ion and the solubility product of $Fe(OH)_{2.70}Cl_{0.30}$ in 0.5 M $(Na^{+})Cl^{-}$ medium. Acta Chemica Scandinavica 20, 1376-1388.

Booth, J., Hong, Q., Compton, R.G., Prout, K., Payne, R.M., 1997. Gypsum overgrowths passivate calcite to acid attack. Journal of Colloid and Interface Science 192, 207-214.

Cravotta, C.A., III, 2008. Dissolved metals and associated constituents in abandoned coal-mine discharges, Pennsylvania, USA. Part 1: Constituent quantities and correlations. Applied Geochemistry 23, 166-202.

Dierick, M., Masschaele, B., Van Hoorebeke, L., 2004. Octopus, a fast and user-friendly tomographic reconstruction package developed in LabView®. Measurement Science and Technology 15, 1366-1370.

Hammarstrom, J.M., Sibrell, P.L., Belkin, H.E., 2003. Characterization of limestone reacted with acid-mine drainage in a pulsed limestone bed treatment system at the Friendship Hill National Historic Site, Pennsylvania, USA. Applied Geochemistry 18, 1705-1721.

Huminicki, D.M.C., Rimstidt, J.D., 2008. Neutralization of sulfuric acid solutions by calcite dissolution and the application to anoxic limestone drain design. Applied Geochemistry 23, 148-165.

Kaufmann, P.R., Herlihy, A.T., Baker, L.A., 1992. Sources of acidity in lakes and streams of the United-States. Environmental Pollution 77, 115-122.

Kepler, D.A., McCleary, E.C., 1994. Successive alkalinity-producing Systems (SAPS) for the treatment of acidic mine drainage. International Land Reclamation and Mine Drainage Conference, Pittsburgh, PA, pp. 195-204.

Nordstrom, D.K., Alpers, C.N., 1999. Geochemistry of acid mine waters. In: Plumlee, G.S., Logsdon, M.J. (Eds.), The Environmental Geochemistry of Mineral Deposits.

Part A. Processes, Methods and Health Issues. Reviews in Economic Geology 6A, 133-160.

Olías, M., Nieto, J.M., Sarmiento, A.M., Cerón, J.C., Cánovas, C.R., 2004. Seasonal water quality variations in a river affected by acid mine drainage: the Odiel River (South West Spain). Science of the Total Environment 333, 267-281.

Parkhurst, D.L., 1995. User's Guide to PHREEQC — A Computer Program for Speciation, Reaction Path, Advective-Transport, and Inverse Geochemical Calculations. US Geological Survey Report WRI no. 95-4227.

Pearson, F.H., McDonnell, A.J., 1975. Use of crushed limestone to neutralize acid wastes. Journal of the Environmental Engineering 101, 139-158.

Rees, B., Bowell, R., Dey, M., Williams, K., 2001. Passive treatment: A walk away solution? Mining Environmental Management, March 2001, 7-8.

Robbins, E.I., Nord, G.L., Savela, C.E., Eddy, J.I., Livi, K.J.T., Gullett, C.D., Nordstrom, D.K., Chou, I.-M., Briggs, K.M., 1996. Microbial and mineralogical analysis of aluminum-rich precipitates that occlude porosity in a failed anoxic limestone drain, Monongalia County, West Virginia. 13th Annual International Pittsburgh Coal Conference, Pittsburgh, p. 761–767.

Rose, A.W., Bisko, D., Daniel, A., Bower, M.A., Heckman, S., 2004. An "autopsy" of the failed Tangaskootack #1 vertical flow pond, Clinton Co., Pennsylvania. Joint Conference of the 21st Annual Meetings of the American Society of Mining and Reclamation and 25th West Virginia Surface Mine Drainage Task Force Symposium, Morgantown, WV, p. 1580-1594.

Rötting, T.S., Caraballo, M.A., Serrano J.A., Ayora, C., Carrera, J., 2008a. Field application of calcite Dispersed Alkaline Substrate (calcite-DAS) for passive treatment of acid mine drainage with high Al and metal concentrations. Applied Geochemistry 23, 1660-1674.

Rötting, T.S., Thomas R.C., Ayora C., Carrera, J., 2008b. Chemical and hydraulic performance of calcite Dispersed Alkaline Substrate (calcite-DAS) for passive treatment of acid mine drainage with high concentrations of Al and Fe. Water Research, in press.

Santomartino, S., Webb, J.A., 2007. Estimating the longevity of limestone drains in treating acid mine drainage containing high concentrations of iron. Applied Geochemistry 22, 2344-2361.

Santoro, L., Volpicelli, G., Caprio, V., 1987. Limestone neutralization of acid waters in the presence of surface precipitates. Water Research 21, 641-647.

Turner, D.R., McCoy, D., 1990. Anoxic alkaline drain treatment system, a low cost acid mine drainage treatment alternative. Proceedings of the 1990 National Symposium on Surface Mining Hydrology, Sedimentology and Reclamation, Lexington, KY, p. 73–75.

Watzlaf, G.R., Kairies, C.L., Schroeder, K.T., Danehy, T., Beam, R., 2002. Quantitative results from the flushing of four Reducing and Alkalinity-Producing Systems. 2002 West Virginia Surface Mine Drainage Task Force Symposium, Morgantown, WV.

Watzlaf, G.R., Schroeder, K.T., Kleinmann, R.L.P., Kairies, C.L., Nairn, R.W., 2004. The Passive Treatment of Coal Mine Drainage. DOE/NETL-2004/1202, U.S. Department of Energy, National Energy Technology Laboratory, Pittsburgh, PA.

Younger, P.L., 2000. The adoption and adaptation of passive treatment technologies for mine waters in The United Kingdom. Mine Water and the Environment 19, 84-97.

Younger, P.L., Banwart, S.A., Hedin, R.S., 2002. Mine Water: Hydrology, Pollution, Remediation. Kluwer Acad. Press, Dordrecht.

Yu, J.-Y., Heo, B., Choi, I.-K., Cho, J.-P., Chang, H.-W., 1999. Apparent solubilities of schwertmannite and ferrihydrite in natural stream waters polluted by mine drainage. Geochimica et Cosmochimica Acta 63, 3407-3416.

Ziemkiewicz, P.F., Skousen, J.G., Simmons, J., 2003. Long-term performance of passive acid mine drainage treatment systems. Mine Water and the Environment 22, 118–129.

Table 1. Parameters and results from the different column experiments. Flux is flow rate per cross-section area per time. τ is the residence time of the solution in the column. It was calculated from flow rates, dimensions and porosities, and ranged from 2 to 20 hours. Concentrations are those of the input solutions (pH 2). All influent solutions were supersaturated with respect to goethite, hematite and schwertmannite (Fe(III)-SO4-H^+ solutions) or akaganeite (Fe(III)-Cl-H^+ solutions). Saturation indices were calculated with the PHREEQC code (Parkhurst, 1995) and the LLNL thermodynamic database included in it. Solubility constants for schwertmannite and akaganeite were from Yu et al. (1999) and Biedermann and Chow (1966), respectively. Influent solutions were stable (no mineral precipitation) before injection into the columns.

Column	Anion	[Fe(III)] (ppm)	[Anion] (mg/l)	Grain size (mm)	Porosity	Flux ($l/m^2/s$)	Diameter (cm)	Length (cm)	Passivation time (h)	t/τ	mg_Fe/ g_calcite
A	SO_4^{2-}	250	1386	2-5	0.44	5.2E-04	6.4	6.0	7030.0	502.3	35.7
B	SO_4^{2-}	1000	3323	1-2	0.47	1.3E-03	2.6	2.5	146.0	59.3	19.2
C	SO_4^{2-}	1000	3323	1-2	0.46	1.4E-03	2.6	2.5	121.9	55.1	17.3
D	SO_4^{2-}	500	2061	1-2	0.48	6.9E-04	2.6	2.5	2443.0	507.5	86.0
F	SO_4^{2-}	1000	3323	2-5	0.43	5.3E-04	4.0	2.3	489.0	94.5	26.3
α	SO_4^{2-}	1000	3323	1-2	0.39	8.0E-04	2.5	2.7	264.0	71.7	17.0
δ	SO_4^{2-}	1000	3323	1-2	0.59	5.7E-04	1.2	1.2	212.0	61.7	33.1
4	Cl^-	1500	2867	2-5	0.48	5.2E-04	6.4	6.0	1174.0	75.2	39.2
7	Cl^-	500	1266	2-5	0.54	5.2E-04	6.4	7.0	5258.1	258.9	56.3
5	Cl^-	1000	2085	2-5	0.48	5.2E-04	6.4	6.0	664.5	43.0	14.7
5*	Cl^-	1000	2085	2-5	0.42	5.2E-04	6.4	5.8	652.2	49.7	13.4
9	SO_4^{2-}	1000	3323	2-5	0.46	5.2E-04	6.4	6.0	344.4	23.3	7.3
11	SO_4^{2-}	1500	4503	2-5	0.46	5.2E-04	6.4	6.0	504.0	34.2	16.0
10	SO_4^{2-}	500	2061	2-5	0.46	5.2E-04	6.4	6.0	3506.0	237.7	37.1

Figure Captions

Figure 1. Schematic diagram of the experimental setup. The lateral sampling ports were only applied to some of the longest columns.

Figure 2. Results from experiment 5*. (a) pH vs. time at the column outlet; (b,c,d,e) pH profiles at different times during the experiment. Times are indicated in (a).

Figure 3. Summary plots of the experimental results. Data are classified into different groups, according to anion, column diameter, flow rate and grain size (O, ×: 1-2 mm; colored solid symbols: 2-5 mm). Lines are only intended to illustrate the trends. (a) Passivation time, normalized to residence time in the column, vs. input Fe(III) concentration; (b) amount of Fe(III) retained, normalized to initial mass of calcite, vs. input Fe(III) concentration; (c) passivation time, normalized to residence time in the column, vs. input SO_4 or Cl concentration; (d) amount of Fe(III) retained, normalized to initial mass of calcite, vs. input SO_4 or Cl concentration. Error bars are calculated from the time between pH measurements at the column outlet (each data point corresponds to the first measurement after the drop in pH; passivation could have occurred at any time after the previous measurement).

Figure 4. SEM image and Fe elemental map from a section from experiment 4 (Fe(III)-Cl-H^+ solution; 1500 ppm Fe). Image width is about 4 mm.

Figure 5. SEM image (backscattered electron) and elemental maps from a section from experiment δ (Fe(III)-SO4-H^+ solution; 1000 ppm Fe). Image width is about 4.5 mm.

Figure 6. XRD profile from precipitates from the uppermost (outlet) part of column 9 (Fe(III)-SO_4-H^+ solution, 1000 ppm Fe). Gypsum and schwertmannite were identified. Red and black vertical lines indicate the peak positions and relative intensities of gypsum ($CaSO_4 \cdot 2H_2O$) and schwertmannite ($Fe_{16}O_{16}(SO_4)_3(OH)_{10} \cdot 10H_2O$), respectively Scan step and scan duration were 0.025^o and 18 s.

Figure 7. X-ray microtomography section of a column (Fe(III)-SO_4-H^+ solution, 1000 ppm Fe). Calcite grains (lighter gray) are coated by gypsum (darker gray). Fe-precipitates are brighter. The formation of preferential pathways for the flow is also evident (non reacted area on the right-hand-side). The inner diameter of the column is 1.2 cm.

Figure 8. (a) Optical micrograph of the sample. Image width is 3.7 mm. Points indicate where measurements were made. (b) XRD profile indicating the presence of goethite in point 3. The two sharp peaks at 35 and 43 degrees came from isolated reflections from a neighboring calcite grain (2D effect).

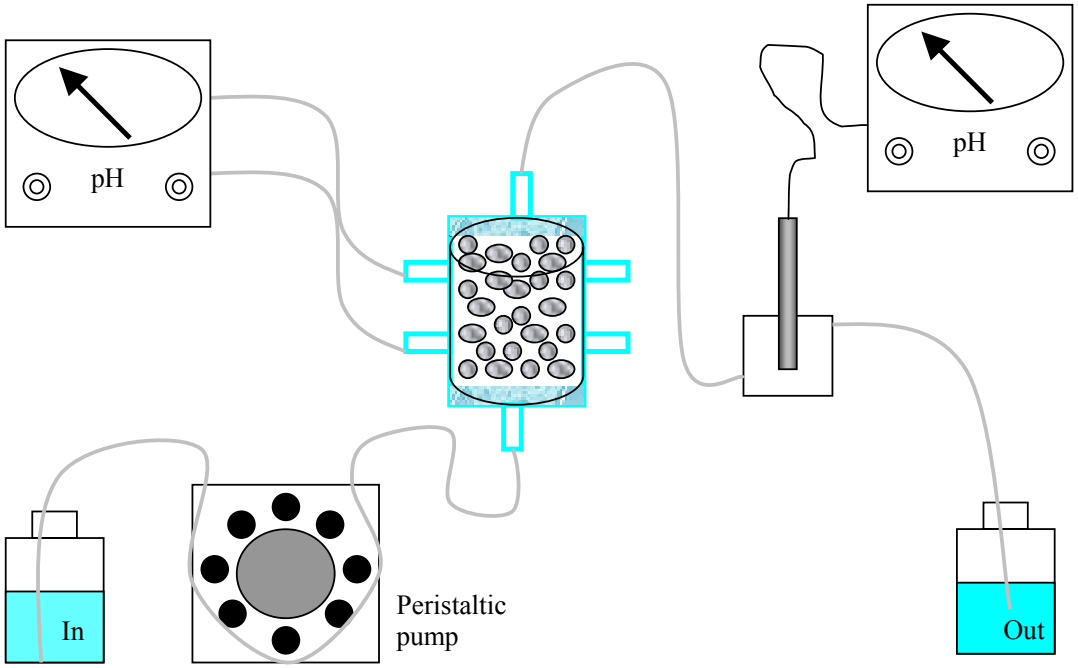

Figure 1

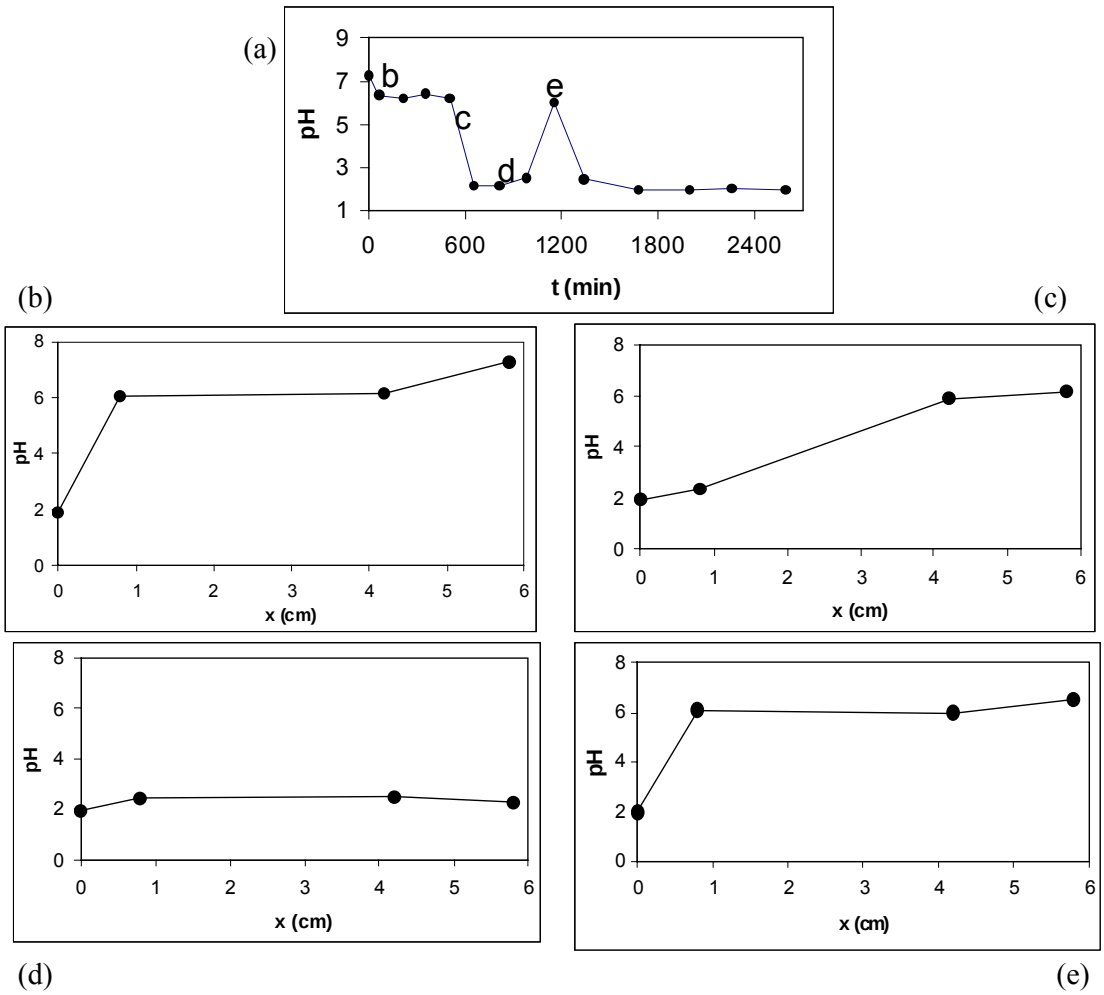

Figure 2

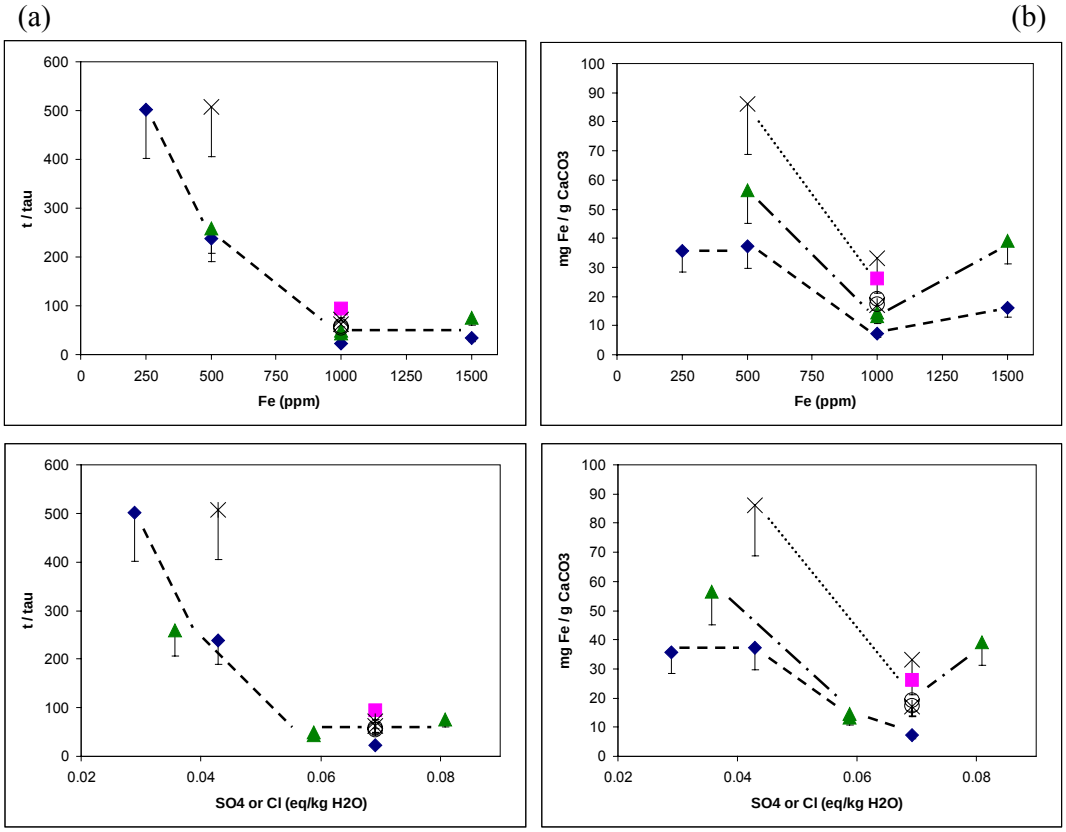

Grain size: 2–5 mm

♦ SO_4, d=6.4 cm, q=5e-4 l/m^2/s

▲ Cl, d=6.4 cm, q=5e-4 l/m^2/s

■ SO_4, d=4.0 cm, q=5e-4 l/m^2/s

Grain size: 1–2 mm

× SO_4, d=1–3 cm, q=6–8e-4 l/m^2/s

O SO_4, d=2.6 cm, q=1.3–1.4e-3 l/m^2/s

Figure 3

(a)

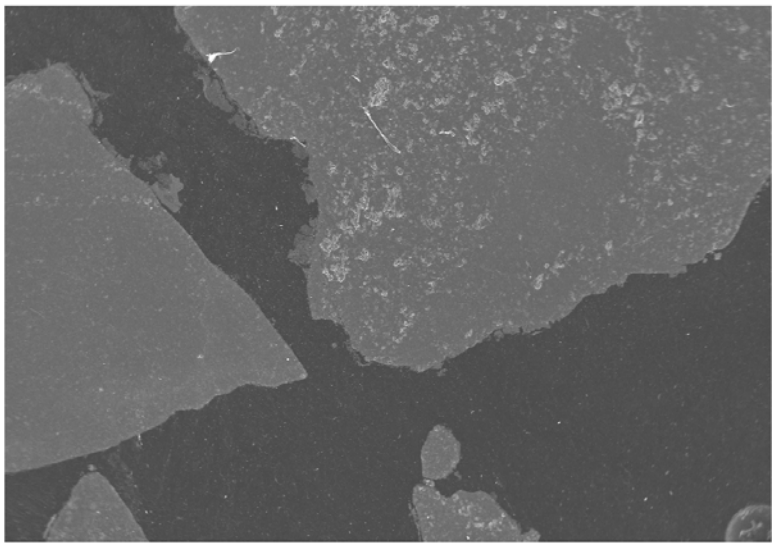

(b)

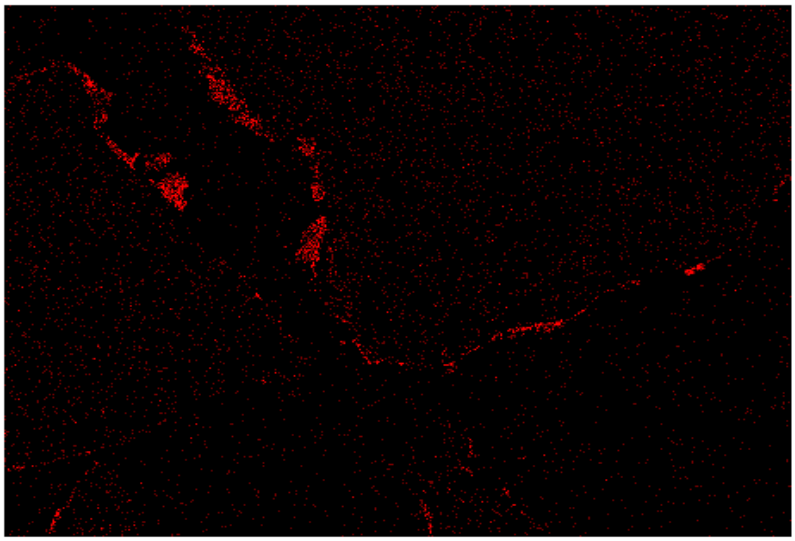

Figure 4

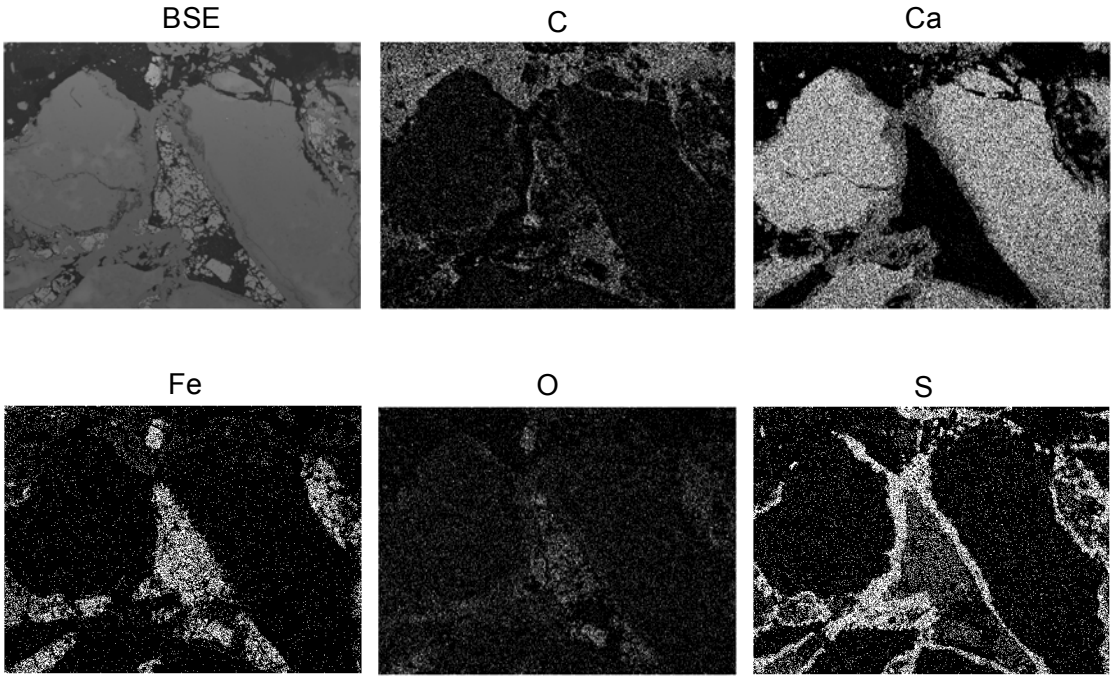

Figure 5

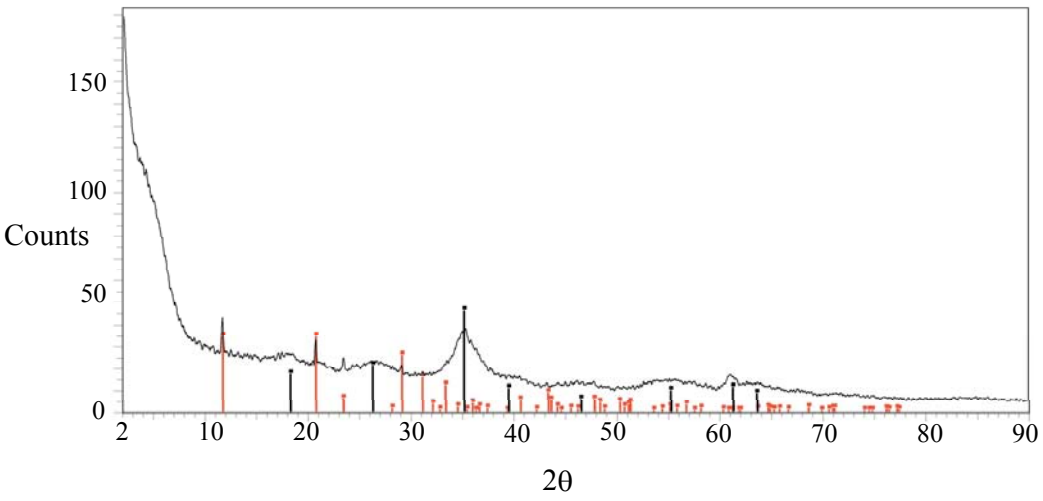

Figure 6

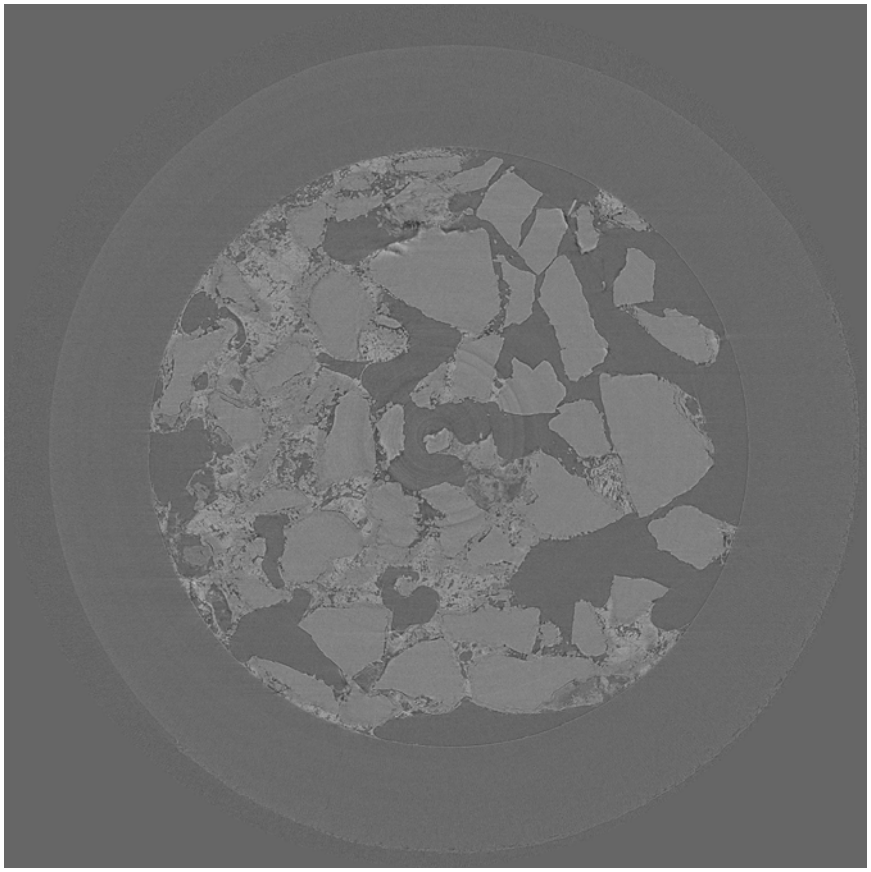

Figure 7

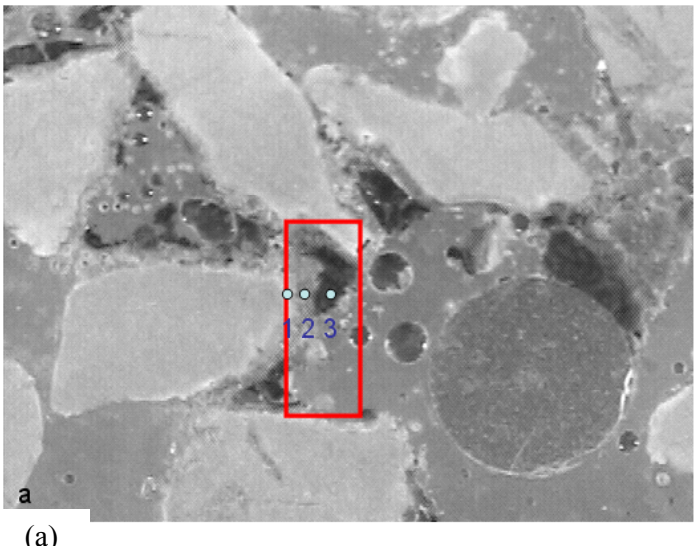
1 2 3
a

(a)

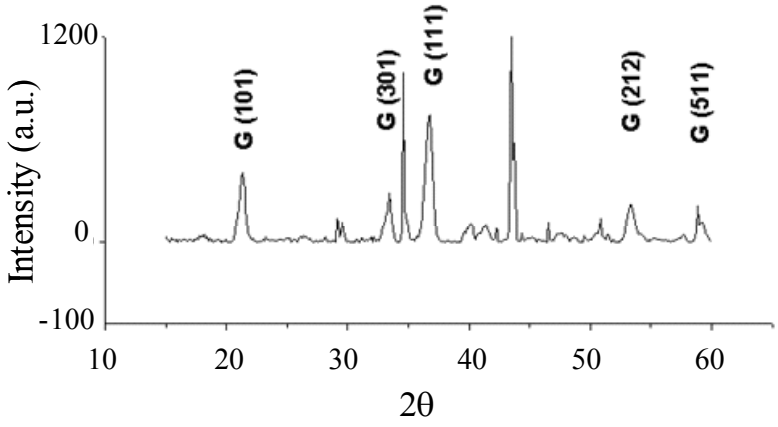
1200
0
-100
Intensity (a.u.)
G (101)
G (301)
G (111)
G (212)
G (511)
10
20
30
40
50
60
2θ

(b)

Figure 8